ISSN 0036-0295, Russian Metallurgy (Metally), Vol. 2022, No. 1, pp. 48–56. © Pleiades Publishing, Ltd., 2022.
Russian Text © The Author(s), 2022, published in Metally, 2022, No. 1, pp. 55–64.

Effect of High-Temperature Pulsed Deuterium Plasma on the Structure and Mechanical Properties of the Surface of Cu–Ga and Cu–Ga–Ni Alloys

I. V. Borovitskaya[a, *], V. N. Pimenov[a, **], S. A. Maslyaev[a, *], A. B. Mikhailova[a, ****], G. G. Bondarenko[b, ********], E. V. Matveev[c, *********], A. I. Gaidar[c], M. Padukh[d, **********], A. S. Demin[a, *****], N. A. Epifanov[a, b, ******], and E. V. Morozov[a, *******]**

[a] *Baikov Institute of Metallurgy and Materials Sciences, Moscow, Russia*
[b] *National Research University Higher School of Economics, Moscow, Russia*
[c] *Research Institute of Advanced Materials and Technologies, Moscow, Russia*
[d] *Institute of Physics of Plasma and Laser Microsynthesis, Warsaw, Poland*
**e-mail: symp@imet.ac.ru*
***e-mail: pimval@mail.ru*
****e-mail: maslyaev@mail.ru*
*****e-mail: sasham1@mail.ru*
******e-mail: casha@bk.ru*
*******e-mail: mophix94@gmail.com*
********e-mail: lieutenant@list.ru*
*********e-mail: gbondarenko@hse.ru*
**********e-mail: niipmt@mail.ru*
***********e-mail: marian.paduch@ifpilm.pl*

Received August 9, 2021; revised August 16, 2021; accepted August 25, 2021

Abstract—The changes in the mechanical properties and the texture of the surface layers in Cu–10Ga and Cu–10Ga–4Ni alloys are studied under the powerful pulsed radiation-thermal and shock-wave loads characteristic of pulsed thermonuclear fusion plants. Samples are irradiated by pulsed high-temperature plasma and ions in the 600-kJ Plasma Focus (PF) PF-1000 (Poland) plant, and deuterium is used as a working gas. The deuterium plasma power density is varied from 10^7 to 10^9 W/cm^2 at the plasma pulse duration of ~10^{-7} s, and the deuterium ion flux power density is from 10^8 to 10^{11} W/cm^2 at an ion flux incident time of ~5×10^{-8} s. Irradiation under the experimental conditions is found to change the texture of the surface layers to a depth of several micrometers, which is likely to be caused by directional solidification at a high temperature gradient oriented normal to the irradiated sample surface. There is a correlation between the type of texture formed in this case and the character of propagating slip lines with formation of a block structure. The lattice parameter in the irradiated surface layers decreases, which is related, supposedly, with the action of residual macroscopic stresses, since substantial changes in the surface layer composition have not been observed. A general tendency toward a decrease in the Vickers microhardness is noted in copper alloy samples as a result of their irradiation in the PF plant under the experimental conditions. A possible cause is thermal effect, since the concentration of alloying elements in the alloys decreases insignificantly after irradiation. The elastic modulus E of the Cu–10Ga alloy decreases insignificantly (to 14%) after irradiation. At the same time, in the Cu–10Ga–4Ni alloy, i.e., after alloying of the Cu–10Ga alloy with nickel (element with higher E as compared to that of copper), the elastic modulus of the initial surface layer remains almost the same after irradiation in PF.

Keywords: copper alloys, pulsed plasma flows, Plasma Focus plant, mechanical properties of surface, texture, slip lines

DOI: 10.1134/S0036029522010050

INTRODUCTION

Copper-base alloys are widely used in many engineering fields due to an appropriate combination of their physicomechanical, electrical properties, and corrosion resistance. These unique characteristics of copper alloys can also be used in thermonuclear reactors (TNRs), in which materials are subjected to pulsed shock-wave and radiation-thermal loads [1]. For example, Cu–Cr–Zr alloys are used in small TNRs, in the systems of active cooling components facing plasma. For the same purpose, an alloy of this

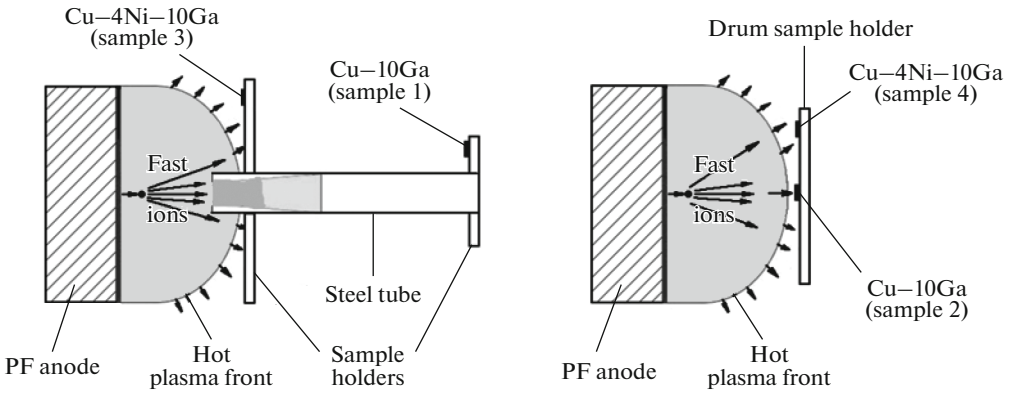

Fig. 1. Block diagram of sample location during irradiation in the PF chamber: (a) experiment 1 and (b) experiment 2.

system was chosen as a material for heat removal elements in the International Thermonuclear Experimental Reactor (ITER) and is the main candidate material in a number of projects of the DEMO reactor [2–4]. The use of copper alloys based on other alloying systems was also considered [5]. Instruments for estimating the resistance of a material under the severe TNR conditions are Plasma Focus (PF) plants, which allow one to model the processes taking place in TNR. The possibility to simultaneously generate powerful flows of high-velocity dense plasma (velocity of ~(2–3) × 10^7 cm/s) and fast ions with energies of several hundreds of keV, short duration of acting pulsed energy fluxes (50–100 ns), and high radiation power densities (to 10^{12} W/cm^2) distinguishes PF plants, which have relative simplicity and a low cost as compared to classical particle and plasma accelerators [6–8].

In addition, under the severe conditions of acting of nanosecond ion, electron, and laser beams on the sample–target surface, shock waves are generated in the material; the passage of these waves changes the structure and the properties of the material. This phenomenon, which is characteristic of pulsed TNRs, can also be modeled using PF plants [9].

This work is a continuation of the studies performed in [10, 11], and its goal is to estimate the changes in the texture and mechanical properties of the surface layers in Cu–10 at % Ga and Cu–10 at % Ga–4 at % Ni alloys under powerful pulsed radiative-thermal and impact loads.

EXPERIMENTAL

We studied Cu–10 at % Ga and Cu–10 at % Ga–4 at % Ni (hereafter, Cu–10Ga and Cu–10Ga–4Ni, respectively) alloys melted in an SShVL-16 vacuum furnace in graphite crucibles; these alloys were represented by the solid solutions of gallium and nickel in copper. The samples were 2-mm-thick pellets 9 mm in diameter.

Irradiation of the samples was carried out in the 600-kJ PF-1000 plant (Poland), and deuterium was used as a working gas at a chamber pressure P = 470 Pa. Two series of experiments were carried out. In the experiment of series 1, samples were fixed near the forward and back ends of a hexagonal tube made of 10Kh12G20V steel so that they were 15 and 40 cm from the anode, respectively (Fig. 1a). In the experiment of series 2, samples were placed on the plasma-facing wall of a drum holder made of Kh18N9T steel and located 12 cm from the anode (Fig. 1b).

In all the experiments, the irradiated target samples were placed near the cathode of the PF chamber. As a result of such an arrangement, only deuterium plasma (DP) acted on sample 1, since the tube wall screened a sample from a fast deuterium ion (DI) flow; however, other samples were irradiated with both DI and DP fluxes. Table 1 gives the irradiation parameters of the alloys in the PF-1000 plant. The energy action on the alloys was varied not only by changing the distances from the anode, but also by a displacement of the alloy samples from the PF chamber axis, since the divergence cone angle of the fast ions generated in PF is ~40° and the body divergence angle of the most powerful ion beam component is only ~7°–10°.

After the experiment, the samples were studied on a Zeiss EVO 40 scanning electron microscope (SEM) equipped with an electron-probe microanalysis (EPMA) attachment, on a Neophot optical metallographic microscope, and an MBS-10 optical microscope.

The X-ray diffraction patterns of the initial samples and the irradiated samples were recorded using Cu$K\alpha$ radiation on a Rigaku Ultima IV X-ray diffractometer (Japan) equipped with a vertical goniometer and a D/teX high-speed semiconductor detector. The detection angle range was 2θ = 38.0°–110.0°, the angular step was 0.02°, and the rate was 2 deg/min. The studies of the phase composition and the determination of the lattice parameters of the samples were

Table 1. Parameters* of irradiation of the experimental alloy samples in the PF-1000 plant

Alloy	Sample	Experiment	L, cm	q_{pl}, W/cm^2	τ_{pl}, s	q_i, W/cm^2	τ_i, s	n
Cu–10Ga	1	1	40	10^7	10^{-7}	–	–	4
	2	2	12	10^9	10^{-7}	10^{11}	5×10^{-8}	9
Cu–10Ga–4Ni	3	1	15	5×10^7–10^8	10^{-7}	10^8–10^9	5×10^{-8}	4
	4	2	12	10^8–10^9	10^{-7}	10^9–10^{10}	5×10^{-8}	5

* L is the distance from the anode, q_{pl} is the DP power density, q_i is deuterium ion D^+ power density, τ_{pl} is the DP pulse duration, τ_i is the deuterium ion D^+ pulse duration, and n is the number of pulses.

carried out using the ICDD Database and the PDXL software.

The microhardness was measured by instrumented indentation (parameters H_{it}, HV*) and the indentation recovery method (HV) on a Shimadzu DUH-211S (Japan) microhardness tester using a diamond Vickers indenter with a squire base (interfacial angle was 136°) according to the standards from [12–15] at a load F_{max} = 50 mN (5.01 Gs) and a holding time of 5 s.

Instrumented indentation is based on continuous recording the dependence of load F on indentation depth h of an indenter into a material and processing of the data obtained on a personal computer (PC) interfaced with a microhardness tester. The measured indentation diagram consists of three sections: loading, holding, and unloading. The data are processed using the Oliver–Pharr technique, which suggests that the contact rigidity changes instantly and constantly in the unloading section. In this case, indentation hardness H_{it} (MPa) is determined from an instrumented indentation diagram as the ratio of the maximum load F_{max} (N) to the projection area A_p (mm^2) of indenter–material contact less the deflection at the indentation edge: $H_{it} = F_{max}/A_p$, where $A_p = 24.5h_c^2$ for the Vickers indenter (in a first approximation), h_c is the contact depth (mm), $h_c = h_{max} - 0.75(h_{max} - h_r)$, h_{max} is the maximum displacement (according to the measured data), and h_r is the intersection of the tangent to the unloading segment at F_{max} with axis h. To compare with available microhardness data, we introduced the "calculated" kinetic Vickers microhardness $HV^* = 0.09453H_{it}$, which is determined using the well-known ratio of the cross-sectional area of the indenter tip $A_p(h_c)$ at a depth h_c to the surface area of the indented part of the indenter $A_s(h)$.

In addition, elastic modulus E_{it} of the alloys before and after irradiation in PF was determined as a result of instrumented indentation. Modulus E_{it} was calculated using the DUXAnalysis module and an analysis of the initial stage of the unloading section, when deformation is purely elastic,

$$E_{it} = \frac{1 - \nu_s^2}{\frac{1}{E_r} - \frac{1 - \nu_i^2}{E_i}},$$

where ν_s and ν_i are the Poisson ratios of the sample material and the indenter, respectively (for diamond, $\nu_i = 0.07$); E_i is the elastic modulus of the indenter (for diamond, E_i = 1140 GPa); E_r is the reduced elastic modulus near the indentation; and $E_r = \sqrt{\pi}/(2C\sqrt{A_p})$, where C is the compliance of the material at the contact determined numerically as $C = dh/dF$ in the unloading section at point F_{max} and $\sqrt{A_p} = 4.950\,h_c$.

Simultaneously, this tester was used to measure Vickers microhardness HV determined from the recovery indentation area: $HV = 189.1F_{max}/L^2$, where F_{max} is the maximum load (mN) and L is the recovered indentation diagonal (μm).

The values of each parameter were found using the results of processing of 15 individual measurements at a confidence coefficient $\alpha = 0.95$. The error of measuring the microhardness on the DUH-211S hardness tester according to GOST 8.904–2015 is not higher than 5%.

RESULTS AND DISCUSSION

Figure 2 shows the typical macrostructure of the sample 2 surface (MBS-10 optical microscope) after irradiation of the Cu–10Ga alloy in the PF plant (Table 1). The irradiated zone has a rounded form; it is surrounded by a breastwork; and there are many melt splashes outside this breastwork.

Table 2 gives lattice parameters a of the initial and irradiated samples of the Cu–10Ga and Cu–10Ga–4Ni (space group $Fm3m$) alloys. It can be noted that, in the initial state, lattice parameter a of the ternary Cu–10Ga–4Ni alloy is slightly smaller than that of the binary Cu–10Ga alloy, which agrees with the data on the decrease in the lattice parameter of pure copper

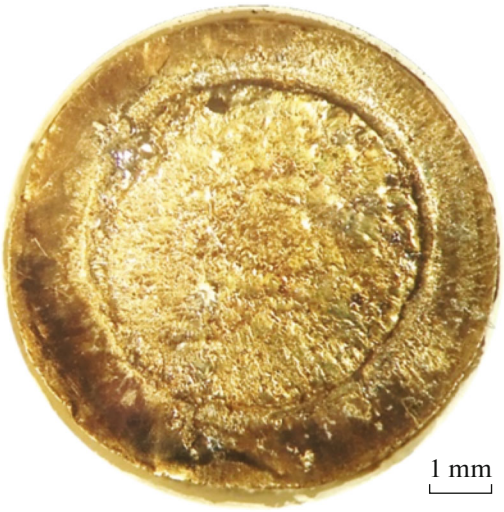

Fig. 2. Typical appearance of the samples after irradiation on the PF plant (sample 2) (photograph was taken in an MBS-10 optical microscope, the sample diameter was 9 mm).

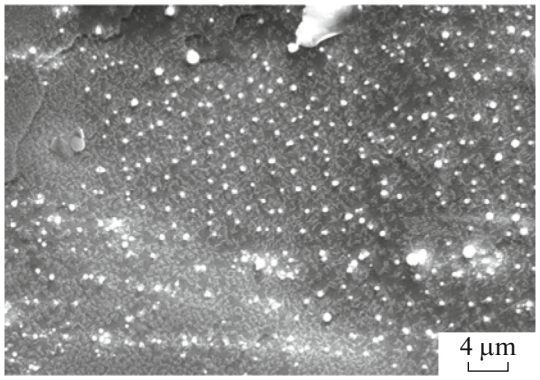

Fig. 3. Microstructure of the Cu–10Ga alloy surface (sample 2) with impurity elements after irradiation in the PF chamber.

when it is alloyed with nickel, which has a smaller atomic radius (1.278 Å for Cu and 1.246 Å for Ni [16]). As follows from an analysis of the data in Table 2, the treatment of the samples by DI and DP fluxes in the PF plant leads to a decrease in parameter *a* in the surface layers (SL) of the copper alloys, and this effect becomes more noticeably when the power of ion–plasma action increases. The exception is sample 2, which was placed immediately at the PF plant axis and was subjected to the strongest energy action. As was shown in [10], the same sample of the Cu–10Ga alloy, unlike other irradiated samples of copper alloys (samples 1, 3, 4 in [10]), undergoes, in parallel with radiation–thermal actions, also the action of shock waves (SWs) generated by powerful pulsed deuterium ion fluxes with a pressure $P = 20$ GPa at the front. The action of shock loads in a combination with thermal stresses favored the formation of plastic deformation in the material and was likely to influence lattice parameter *a* (Table 2). In addition, the EPMA studies of the surface structure and composition performed on a SEM showed that the elements that existed in the PF chamber materials, mainly sulfur, deposited onto the sample–target surface with formation of metal sulfides during irradiation (Fig. 3). The existence of sulfur is most likely to be related to its evaporation from the surfaces of the sulfur-containing functional materials of the PF chamber. The presence of these impurities can also influence the lattice parameter of sample 2 as a result of their dissolution in the alloy and deeper penetration into the material under action of SWs.

The processes leading to a decrease in the lattice parameter after irradiation could be related to the evaporation of gallium as a low-melting element, which increases parameter *a* [17]. However, the EPMA results showed that there is no marked (higher than the measurement error) decrease in its concentration in a 1-μm layer (analyzed layer depth according to EPMA) (Table 3). At the same time, the authors of [18–21] detected a more substantial decrease in parameter *a* during ion–plasma treatment of vanadium, titanium, zirconium, and their alloys. This effect was assumed to be related to the action of residual macrostresses and a change in the elemental composition in the surface layers of the samples. In our case, the small decrease in the lattice parameter after irradiation is also assumed to be caused by the action of residual macrostresses.

Figures 4a and 4b show the X-ray diffraction patterns of the Cu–10Ga and Cu–10Ga–4Ni alloys before and after irradiation by radiation fluxes in PF and also present X-ray diffraction data for the ($Cu_{0.875}Ga_{0.115}$) compound from the ICDD database with the ratio of the line intensities corresponding to a reference sample (Fig. 4c). Note the existence of (200) texture in the initial (as-cast) state in the Cu–10Ga alloy, which can be removed by additional recrystallization annealing. The formation of a sharp texture in sample 3 (Cu–10Ga–4Ni alloy) in the (111) direction

Table 2. Lattice parameters of the alloys after irradiation under various conditions*

Alloy	Sample	*a*, Å
Cu–10Ga	Ini.	3.641(5)
	1	3.639(7)
	2	3.642(6)
Cu–10Ga–4Ni	Ini.	3.637(5)
	3	3.636(4)
	4	3.635(7)

* Samples: 1–4.

Table 3. Contents of the main elements in the surface layers of Cu–10Ga and Cu–10Ga–4Ni alloys after irradiation under various conditions

Alloy	Sample	Elemental content					
		wt %			at %		
		Cu	Ga	Ni	Cu	Ga	Ni
Cu–10Ga	Ini.	90.32 ± 2.56	9.68 ± 0.56	–	91.10	8.90	–
	1	90.15 ± 2.25	9.85 ± 0.42	–	90.94	9.06	–
	2	90.56 ± 2.25	9.44 ± 0.38	–	91.32	8.68	–
Cu–10Ga–4Ni	Ini.	86.33 ± 2.37	9.84 ± 0.43	3.83 ± 0.17	86.81	9.02	4.17
	3	86.74 ± 2.28	8.77 ± 0.37	4.49 ± 0.19	87.09	8.03	4.88
	4	86.67 ± 2.08	9.06 ± 0.29	4.27 ± 0.14	87.06	8.29	4.64

The error in determining the element content is given according to the readings of an EVO 40 device.

caused, most likely, by directional solidification at a high temperature gradient oriented normal to the irradiated surface is noteworthy. The X-ray diffraction patterns of metallic alloys recorded using a copper anode mainly characterize the structure of the surface and near-surface layers to a depth of several micrometers, and we can conclude that the (111) texture in sample 3 propagate at least to this depth.

Metals with an fcc lattice, among them is copper, are known to have 12 slip systems along the {111} planes and in the ⟨110⟩ directions (with the closest packing). Since a sharp (111) texture, which is a slip plane, appeared in sample 3, it is likely to explain the plastic flow particularly developed in this sample with the formation of a block structure under thermomechanical stresses and observed in [11]. To a lesser degree, this effect was observed in sample 4 of the same alloy, but the number of slip lines in the Cu–10Ga alloy (samples 1 and 2), in which the texture is weak or is almost absent, is substantially smaller.

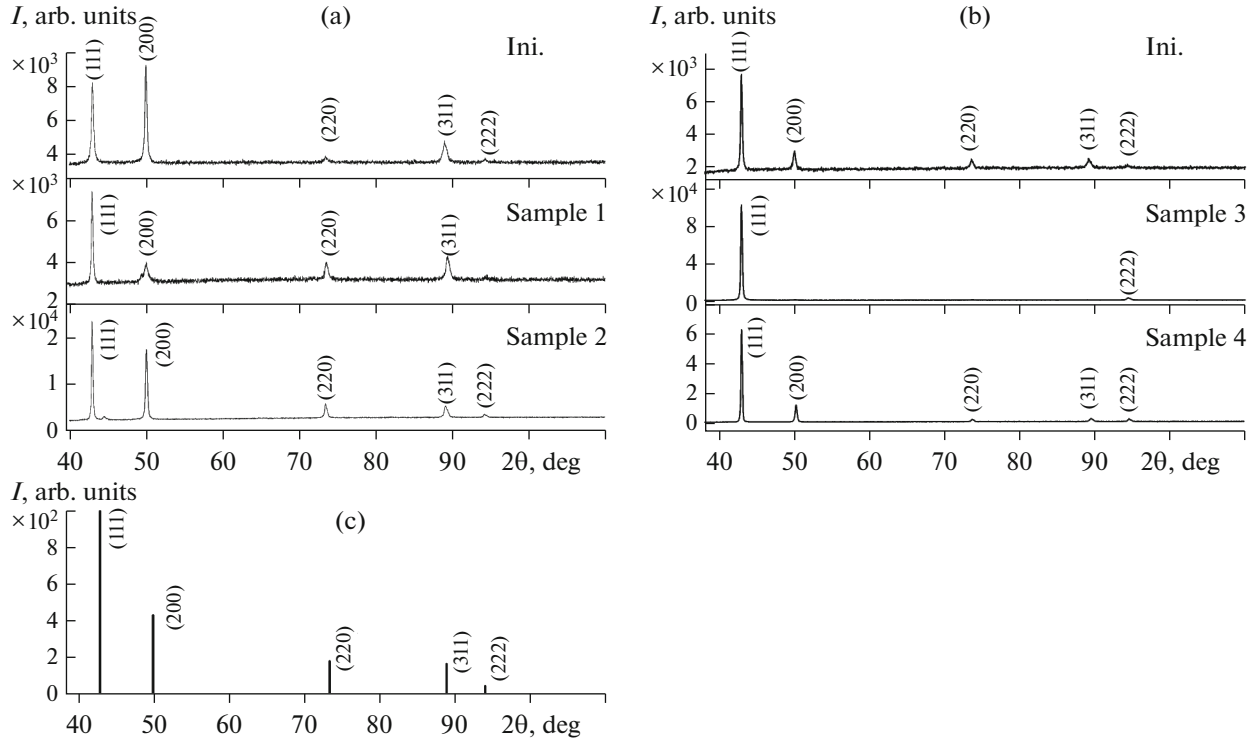

Fig. 4. X-ray diffraction patterns of (a) Cu–10Ga and (b) Cu–10Ga–4Ni alloys and (c) X-ray diffraction data for the $Cu_{0.875}Ga_{0.115}$ compound from the ICDD Database with the ratio of the line intensities corresponding to the reference sample.

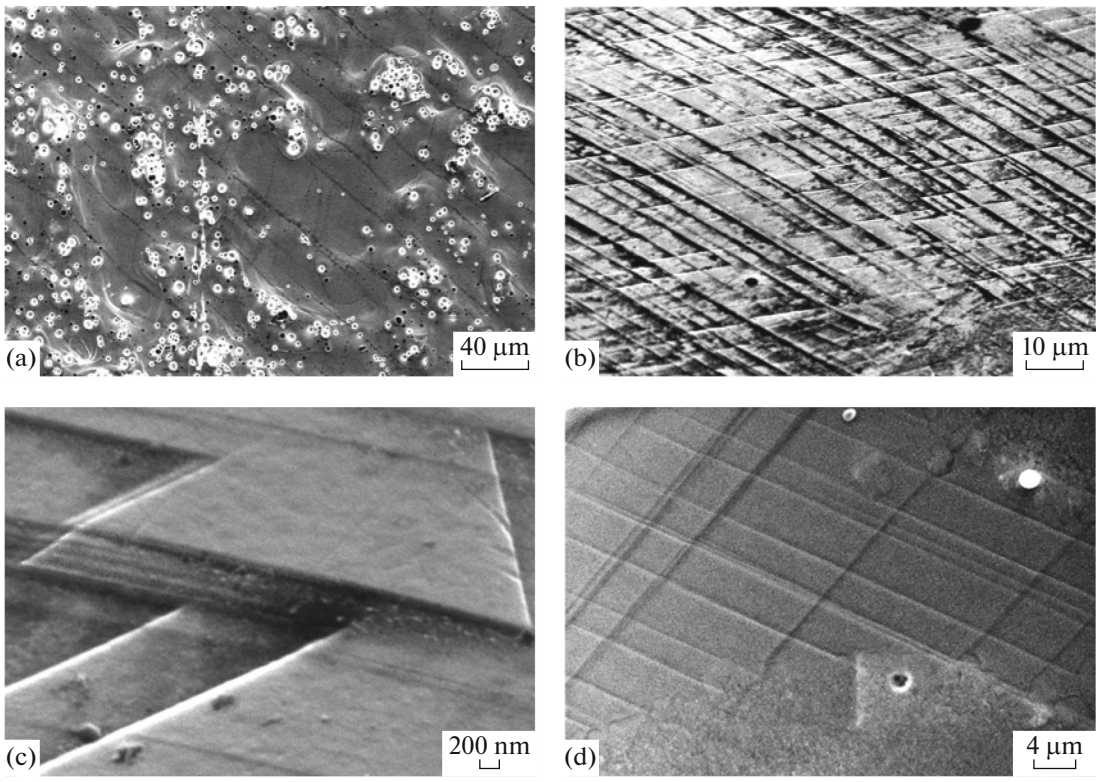

Fig. 5. Microstructures of (a) Cu–10Ga and (b–d) Cu–10Ga–4Ni alloys after irradiation in the PF plant under various conditions: (a) sample 1, (b, c) sample 3 at various magnifications, and (d) sample 4.

Figure 5 shows photographs of the microstructures, which illustrate the effects described above.

The studies of changing the strength properties of the surface layers (SLs) of materials, particularly microhardness, due to their irradiation in a PF plant are interesting for the determination of their fracture resistance under the extreme thermal and radiation actions occurring in TNR. In addition, similar treatment of materials with pulsed energy fluxes can be a promising method for modifying the properties of their SLs.

When studying the microhardness, it is important to choose the maximum indenter load F_{max}, since it is known that the micro- and nanohardnesses can be different in a certain range of F_{max} values (scale factor). In [22], the nanohardness of a single-crystal Cu (111) copper was studied as a function of load F_{max}, and a decrease in F_{max} was shown to increase in the nanohardness. However this effect is observed fairly noticeably at $F_{max} < 40$ mN and particularly strongly at $F_{max} < 6$ mN. In our case, we use a load $F_{max} = 50$ mN (5.01 gf), which is higher than the above values.

Figure 6 shows the results of measuring the Vickers microhardness by two methods: using a recovered indentation (*HV*) and instrumented indentation (*HV**). In the case of instrumented indentation, the microhardness is calculated as the ratio of the load to the surface area of an unrecovered indentation expressed via its depth. This method has an advantage on testing materials with high elastic properties, which significantly decrease the indentation sizes after unloading.

As is seen from Fig. 6, the microhardness determined from a recovered indentation is slightly lower than the kinetic hardness; however, the situation appears to be the opposite, since the recovered indentation has a smaller size. The same regularity was observed during the measurements on a reference sample made of unalloyed copper: $HV^* = 149.4 \pm 12.9$, $HV = 119.9 \pm 3.3$ kgf/mm^2.[1]

This effect can be explained using the results of [23], where the Vickers hardness measured by instrumented indentation on a Fisherscope HM2000 device was compared with the hardness measured by the recovered indentation method on the same instrument and also on an HMV microhardness tester. The kinetic hardness was 6–10% higher than that obtained by the recovered indentation method. The authors explained the higher values of Vickers hardness obtained by instrumented indentation mainly by the peculiarity of determining the area using the values of the total indentation depth h_{max} and the indentation

[1] The coefficient of reducing these results to the SI units is 1 kgf/mm^2 ≈ 10 MPa.

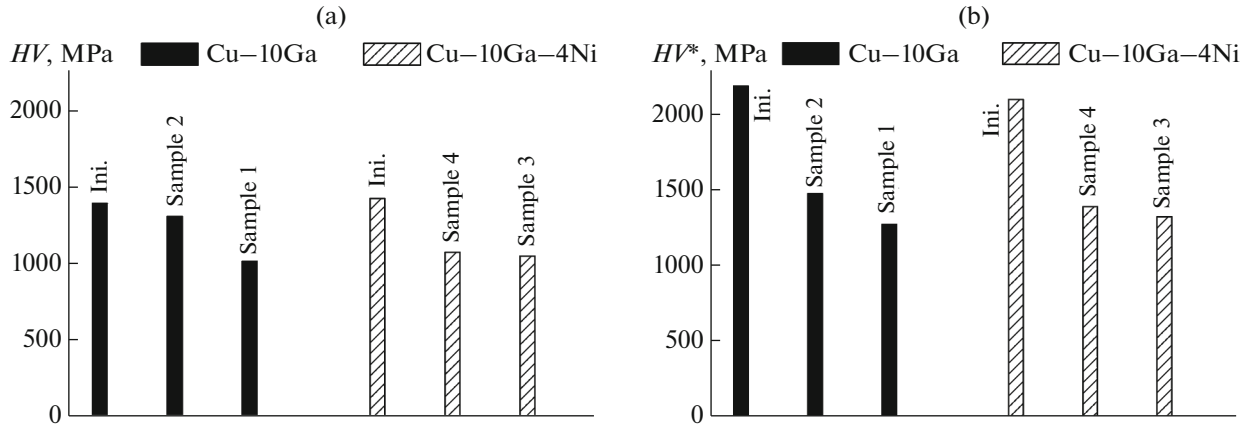

Fig. 6. Microhardnesses of Cu–10Ga and Cu–10Ga–4Ni alloys in the initial state and after treatment in the PF plant: (a) Vickers hardness (from recovered indentation) and (b) kinetic hardness. Load on indenter was $P = 0.05$ N (5 gf).

depth after unloading h_r, when the areas determined by h_{max} and h_r are overestimated in the first case and underestimated in the second case. The averaged correlation dependences, which are used finally to determine the Vickers hardness, also contribute to the difference between the results, when instrumented indentation is used. To decrease the measurement error, correlation dependences should be built independently and individually for each material and its state.

The copper alloys studied in this work demonstrate a general tendency to decrease the microhardness after irradiation in the PF chamber. A possible cause is a thermal influence, since, as was noted above, the gallium concentration in the surface layer after PF decreases insignificantly, and it is unlikely that this fact strongly influences *HV*. At the same time, conversely, in some other works, e.g., [18], the hardening of the surface layer of vanadium when irradiated with nitrogen plasma in a PF plant was observed; this effect correlates with refining CDS (coherent domain size) blocks, increasing the lattice microstrain ε, and the formation of vanadium nitrides. An increase in the microhardness of titanium after irradiation with nitrogen plasma under similar conditions was also observed in [19]. Thus, the particular influence of radiation-thermal treatment in a PF plant on the strength properties of irradiated SL is dependent on the combination target–irradiation conditions.

Table 4. Elastic moduli of Cu–10Ga and Cu–10Ga–4Ni alloys determined by instrumented indentation and the average indentation depth h_{av}

Alloy	Sample	E, GPa	h_{av}, μm
Cu–10Ga	Ini.	112.53 ± 3.6	1.03 ± 0.15
	1	96.5 ± 6.2	1.32 ± 0.04
	2	97.0 ± 10.8	1.24 ± 0.27
Cu–10Ga–4Ni	Ini.	116.9 ± 7.2	1.04 ± 0.13
	3	114.0 ± 9.3	1.28 ± 0.08
	4	115.6 ± 15.4	1.26 ± 0.09

Figure 7 shows the typical indentation curves of the Cu–10Ga and Cu–10Ga–4Ni alloys in the initial state and after treatment in PF. It is seen that the curves of loading and unloading have no any steps and kinks, which shows that the zone depth in which melting and solidification take place is larger than the depth to which indenter penetrates (as average, to 1.32 μm, Table 4).

It is also interesting to determine the change in the elastic moduli as a result of pulsed treatment of the alloy samples with fluxes of ions and pulsed high-temperature plasma. This is important due to the fact that a possible difference of the elastic moduli of a modified surface layer and the crystal substrate will cause, when loading a material (for example, under action of SWs or thermal shock), the formation at the interface of strong tensile and compressive normal stresses and related strains. These stresses can favor the development of plastic flow in a remelted layer of the copper alloy and lead to a damage and fracture of surface layer in more brittle materials such as tungsten and molybdenum.

To control the correctness of determining the elastic moduli by indentation with a diamond pyramid, we determined the values of E of the reference sample (copper plate) by two methods: in the tensile test (by the initial segment of the stress–strain diagrams) and in the indentation tests (using a Shimadzu DUH-211S tester). We obtained $E = 114.3$ GPa in the first case, and $E_{it} = 122.8$ GPa in the second case; i.e., the difference is no higher than 10% and can be explained by both the difference in the methods used and also by the fact that, in the first case, the modulus is determined in the sample bulk and, in the second case, in a thin surface layer with thickness of 1.00–1.32 μm

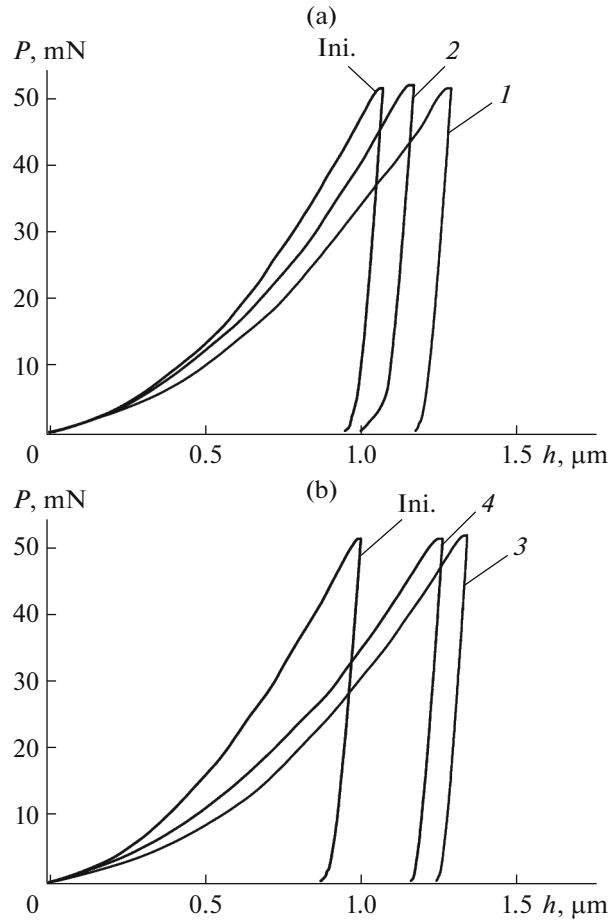

Fig. 7. Typical indentation curves of (a) Cu–10Ga and (b) Cu–10Ga–4Ni alloys in the initial state and after treatment of samples 1–4 in the PF plant (*h* is the indentation depth).

(Table 4), which can slightly differ from the bulk, for example, by the texture.

As a result of determination of the elastic moduli of the alloys under study, given in Table 4, it can be noted that, in the initial state, the difference between the moduli *E* of the Cu–10Ga and Cu–10Ga–4Ni alloys is no higher than the measurement error. After treatment of the materials to be compared in the PF plant, the elastic modulus decreases by 13–14% in samples 1 and 2 (Cu–10Ga alloy), and modulus *E* of samples 3 and 4 (Cu–10Ga–4Ni alloy) is changed only slightly after irradiation. This result is likely to be due to the effect of alloying of the Cu–10Ga alloy with nickel, modulus *E* of which is higher than that of copper.

CONCLUSIONS

(1) Samples of alloys Cu–10 at % Ga and Cu–10 at % Ga–4 at % Ni (Cu–10Ga and Cu–10Ga–4Ni, respectively) were irradiated in the PF-1000 plant (further, PF) with pulsed fluxes of high-temperature deuterium plasma with a power density $q_p = 10^7$–10^9 W/cm^2 at a pulse duration $\tau_m = 10^{-7}$ s and deuterium ions with a power density $q_i = 10^8$–10^{11} W/cm^2 at $\tau_i = 5 \times 10^{-8}$–$10^{-7}$ s. X-ray diffraction studies showed that the ion-plasma treatment of the alloys in the PF plant slightly decreased the lattice parameter in the irradiated surface layers, and this effect becomes more noticeable as the pulsed energy flux power increases. This fact is likely to be related to the influence of residual macrostresses, since no changes in the surface layer composition were observed.

(2) The hard irradiation conditions of a Cu–10Ga alloy sample in the PF plant, which are accompanied by the deposition on the sample–target of elements of the functional materials that exist in the PF chamber and action of SWs on the alloy, lead to some increase in the lattice parameter in the surface layer of the copper-based solid solution. The observed effect is likely to be related to the dissolution of the deposited elements in the surface layer in combination with the action of SW loads on the material, which favor their penetration into the alloy.

(3) The texture in the surface layers of the irradiated samples was found to change to a depth of several micrometers, which is likely due to directional solidification at a high temperature gradient oriented normal to the irradiated sample surface. There is a correlation between the type of formed texture and the character of propagation of slip lines with formation of a block structure.

(4) There is general tendency to decrease the Vickers microhardness (both kinetic microhardness and microhardness determined from a recovered indentation) of the copper alloy samples as a result of irradiation in the PF plant under the experimental conditions. A possible cause is a thermal effect leading to melting and solidification of the surface layer, because the concentration of alloying elements in it decreases insignificantly after irradiation.

(5) An analysis of the indentation curves shows that the zone depth, in which melting and solidification take place during irradiation in the PF plant, is larger than 1.3 μm. The decrease in the elastic modulus observed in the Cu–10Ga alloy after irradiation is not higher than 14%. When this alloy is alloyed with nickel (Cu–10Ga–4Ni alloy), i.e., an element whose elastic modulus is higher than that of copper, the elasticity of the initial surface layer remains almost unchanged after irradiation of the material in PF plant under the experimental conditions.

FUNDING

This work was carried out in the framework of state task no. 075-00328-21-00 and was supported by the International Atomic Energy Agency, contract no. 23664.

CONFLICT OF INTEREST

The authors declare that they have no conflicts of interest.

REFERENCES

1. M. L. Subbotin, D. K. Kurbatov, and E. A. Filimonova, "Review of states of studies of demonstration thermonuclear reactors in the world," Vopr. At. Nauki Tekh., Ser. Termoyad. Sint., No. 3, 55–74 (2010).
2. A. Hernández-Pérez, M. Eddahbi, M. A. Monge, A. Muñoz, and B. Savoini, "Microstructure and mechanical properties of an ITER-grade Cu–Cr–Zr alloy processed by equal channel angular pressing," Fusion Eng. Des. **98**–**99**, 1978–1981 (2015).
3. J. Y. Park, Y. Il. Jung, B.-K. Choi, J.-S. Lee, Y. H. Jeong, and B. G. Hong, "Investigation on the microstructure and mechanical properties of CuCrZr after manufacturing thermal cycle for plasma facing component," J. Nucl. Mater. **417**, 916–919 (2011). https://doi.org/10.1016/j.jnucmat.2010.12.157
4. A. J. Cackett, J. J. H. Lim, P. Klups, A. J. Bushby, and C. D. Hardie, "Using spherical indentation to measure the strength of copper–chromium–zirconium," J. Nucl. Mater. **511**, 610–616 (2018).
5. S. J. Zinkle, "Applicability of copper alloys for DEMO-high heat flux components," Phys. Scripta **167**, 014004 (2016). https://doi.org/10.1088/0031-8949/2015/T167/014004
6. V. A. Gribkov, F. I. Grigor'ev, B. A. Kalin, and V. L. Yakushin, *Advanced Radiation-Beam Technologies of Processing Materials* (Kruglyi God, Moscow, 2001).
7. V. A. Gribkov, "Physical processes taking place in dense plasma focus devices at the interaction of hot plasma and fast ion streams with materials under test," Plasma Phys. Control. Fusion **57** (6) (2015). https://doi.org/10.1088/0741-3335/57/6/065010
8. V. A. Gribkov, I. V. Borovitskaya, A. S. Demin, E. N. Morozov, S. A. Maslyaev, V. N. Pimenov, A. V. Golikov, A. K. Dulatov, G. G. Bondarenko, and A. I. Gaidar, "Plasma Focus Vikhr' plant for diagnostics of the radiation-thermal resistance of materials promising for the thermonuclear energetic and aerospace engineering," Prib. Tekh. Eksp., No. 1, 75–83 (2020). https://doi.org/10.31857/S0032816219060193
9. S. V. Latyshev, V. A. Gribkov, S. A. Maslyaev, V. N. Pimenov, M. Padukh, and E. Zhelin'ska, "Generation of shock waves in materials-science experiments on Plasma Focus plants," Perspek. Mater., No. 1, 5–12 (2014).
10. I. V. Borovitskaya, V. A. Gribkov, A. S. Demin, N. A. Epifanov, S. V. Latyshev, S. A. Maslyaev, E. V. Morozov, V. N. Pimenov, I. P. Sasinovskaya, G. G. Bondarenko, A. I. Gaidar, and M. Sholtz, "Damageability and deformation effects in surface layers of copper and copper-gallium alloys under pulsed irradiation in the Plasma Focus plant," Perspek. Mater., No. 5, 23–37 (2020). https://doi.org/10.30791/1028-978X-2020-5-23-37
11. V. N. Pimenov, I. V. Borovitskaya, V. A. Gribkov, A. S. Demin, N. A. Epifanov, S. A. Maslyaev, E. V. Morozov, I. P. Sasinovskaya, G. G. Bondarenko, A. I. Gaidar, and M. Padukh, "Effect of pulsed fluxes of deuterium ions and deuterium plasma on copper-nickel and copper-nickel-gallium alloys," Poverkhnost, No. 1 (2021).
12. *GOST P 8.748–2011 (ISO 14577-1: 2002). Metals and Alloys. Measurement of the Hardness and Other Characteristics of Materials upon Instrumented Indentation* (Standartinform, Moscow, 2013).
13. *GOST 8.904–2015 (ISO 14577-2: 2015). Measurement of the Hardness and Other Characteristics of Materials upon Instrumented Indentation* (Standartinform, Moscow, 2016).
14. *GOST P ISO 6507-1–2007. Metals and Alloys. Measurement of the Vickers Hardness: Part 1. Measurement Method* (Standartinform, Moscow, 2008).
15. *GOST 9450–76. Microhardness Measurement by Indentation of Diamond Indenter* (Izd. Standartov, Moscow, 1993).
16. P. Villars, K. Brandenburg, M. Berndt, S. LeClair, A. Jackson, Y.-H. Pao, B. Igelink, M. Oxley, B. Bakshi, P. Chen, and S. Iwata, "Binary, ternary, and quaternary compound former/nonformer prediction via Mendeleev number," J. Alloys Compd. **317**, **318**, 26–38 (2001).
17. A. E. Vol, *Structure and Properties of Binary Metallic Systems* (Fizmatlit, Moscow, 1962), Vol. 2.
18. I. V. Borovitskaya, V. Ya. Nikulin, G. G. Bondarenko, A. B. Mikhailova, P. V. Silin, A. I. Gaidar, V. V. Paramonova, and E. N. Peregudova, "Effect of pulsed nitrogen plasma and nitrogen ion fluxes on the structure and mechanical properties of vanadium," Russ. Met. (Metally), No. 3, 266–275 (2018).
19. V. N. Pimenov, V. V. Roshchupkin, S. A. Maslyaev, et al., "Surface effects caused by action of pulsed fluxes of nitrogen ions and nitrogen plasma on a Ti–Al alloy," Perspek. Mater., No. 4, 77–85 (2011).
20. M. M. Grekhov, "Structural and textural changes induced by ion–plasma irradiation in Zr-based alloys and determined by X-ray diffraction," *Extended Abstract of Cand. Sci. (Phys.–Math.) Dissertation*, Inst. Eng. Phys., Moscow, 2009.
21. Yu. A. Perlovich, M. G. Isaenkova, M. M. Grekhov, V. V. Fesenko, B. A. Kalin, and V. L. Yakushin, "Change in the structure and texture in the volume of cladding tubes made of a zirconium-based alloys upon the ion-plasma treatment of the surface," Vopr. At. Nauki Tekh., Ser. Fiz. Radiats. Povrezhd. Radiats. Materialoved., No. 3 (85), 59–65 (2004).
22. Yu. V. Mil'man, A. A. Golubenko, and S. N. Dub, "Determination of the nanohardness at a fixed indentation size to eliminate a scale factor," Vopr. At. Nauki Tekh., No. 2 (96), 171–177 (2015).
23. R. A. Vorob'ev, V. N. Litovchenko, and V. N. Dubinskii, "Instrumented indentation study of the hardness and the elastic modulus of ferrite," Zavod. Lab. **82** (5), 55–60 (2016).

Translated by Yu. Ryzhkov